

Shear jamming, discontinuous shear thickening, and fragile state in dry granular materials under oscillatory shear

Michio Otsuki^{1,*} and Hisao Hayakawa²

¹ Graduate School of Engineering Science, Osaka University, Toyonaka, Osaka 560-8531, Japan

² Yukawa Institute for Theoretical Physics, Kyoto University,
Kitashirakawaoiwake-cho, Sakyo-ku, Kyoto 606-8502, Japan

(Dated: October 10, 2018)

The mechanical response of two-dimensional frictional granular materials under an oscillatory shear are numerically investigated. It is confirmed that the shear storage modulus G' depends on the initial amplitude of the oscillation to prepare the system before the measurement. For sufficiently large initial strain amplitude, the shear jammed state satisfying $G' > 0$ is observed even if the packing fraction is below the jamming point. The fragile state is also identified as a long lived metastable state where G' depends on the phase of the oscillatory shear. The dynamic viscosity evaluated from the shear loss modulus G'' exhibits a sudden jump similar to the discontinuous shear thickening in the fragile state.

PACS numbers: 45.70.-n, 05.70.Jk, 81.40.Jj

Introduction.— Amorphous materials consisting of repulsive and dissipative particles such as granular materials, colloidal suspensions, foams, and emulsions can form solid-like jammed states. Since Liu and Nagel suggested that jammed states exist only above a critical packing fraction ϕ_J [1], the jamming transition has attracted much attention among physicists [2, 3]. Several numerical simulations of frictionless grains support this picture and reveal various critical behaviors near ϕ_J , where the pressure and the coordination number exhibit continuous and discontinuous transitions, respectively [4–6]. Continuous transitions are also observed for rheology of frictionless particles under steady shear [7–29] and oscillatory shear [30, 31].

Nevertheless, granular particles cannot be free from mutual frictions between grains, which play crucial roles in the dynamics of granular materials. Indeed, recent experiments suggest frictional grains follow a different scenario from that of frictionless grains, i.e. jammed states for frictional grains are induced by shear deformation even below ϕ_J [32]. Such a transition, known as shear jamming has been studied experimentally [33–35] and numerically [36, 37]. In Ref. [32], the shear jammed state is characterized by the percolation of an isotropic force network, while the fragile state characterized by an anisotropically percolated network is also found.

It is also known that mutual frictions between grains cause drastic changes of the rheology such as the discontinuous shear thickening (DST) [38–61], which is applied to flexible protective gears [62] and robotic manipulators [63]. There have been various studies focusing on the relationship between DST and the shear jamming in suspensions of frictional grains under steady shear [53–56]. The conclusions as well as the definitions of the shear jamming, however, are inconsistent with each

other. Moreover, the definition of the fragile state is still controversial [32, 53]. Therefore, we have to clarify the relationship between the mechanical response and the shear jammed state or the fragile state in granular materials.

To resolve the above puzzled situation, we numerically study the mechanical response of two-dimensional frictional grains near the jamming transition under oscillatory shear. We find that the shear jamming, the DST, and the fragile state depend on the amplitude of the oscillatory shear before measuring mechanical properties. The shear jammed state satisfying the shear storage modulus $G' > 0$ can be observed for the packing fraction $\phi < \phi_J$ above a critical strain amplitude. We also confirm that the observable region for a DST-like behavior is identical to that of the fragile state: a long-lived metastable state depending on the phase of the oscillatory shear.

Setup of Simulation.— Let us consider a two-dimensional assembly of N frictional granular particles. They interact according to the Cundall-Strack model with an identical mass density ρ in a square periodic box of linear size L [64]. The normal repulsive interaction force $F^{(n)}$ is given by $F^{(n)} = F^{(n,el)} + F^{(n,vis)}$, where $F^{(n,el)} = k^{(n)}r$ and $F^{(n,vis)} = -\eta^{(n)}\dot{r}$ with the compression length r , the compression velocity \dot{r} , the normal spring constant $k^{(n)}$, and the normal viscous constant $\eta^{(n)}$. The tangential contact force $F^{(t)}$ is given by $F^{(t)} = \min\left(|\tilde{F}^{(t)}|, \mu F^{(n,el)}\right) \text{sgn}\left(\tilde{F}^{(t)}\right)$, where $\min(a, b)$ selects the smaller one between a and b , $\text{sgn}(x) = 1$ for $x \geq 0$ and $\text{sgn}(x) = -1$ otherwise, and $\tilde{F}^{(t)}$ is given by $\tilde{F}^{(t)} = k^{(t)}\delta^{(t)} + \eta^{(t)}\dot{\delta}^{(t)}$. Here, $k^{(t)}$ and $\eta^{(t)}$ are the elastic and viscous constants in the tangential direction, respectively. The tangential displacement $\delta^{(t)}$ is given by $\delta^{(t)} = \int_{\text{stick}} dt \dot{\delta}^{(t)}$ with the tangential velocity $\dot{\delta}^{(t)}$, where “stick” on the integral indicates that the integral is performed when the condition $|\tilde{F}^{(t)}| < \mu F^{(n,el)}$ is satisfied. To avoid crystallization, we use a bi-disperse system which includes equal number of grains of the diameters

*otsuki@me.es.osaka-u.ac.jp

d_0 and $d_0/1.4$, respectively.

In this system, we apply an oscillatory shear along the y direction under the Lees-Edwards boundary condition with the SLLOD algorithm which stabilizes a bulk shear state [65]. As an initial state, the disks are randomly placed in the system with the initial packing fraction $\phi_I = 0.75$, and we slowly compress the system until the packing fraction reaches a given value ϕ as shown in Ref. [61]. After the compression, the shear strain is applied as $\gamma(t) = \gamma_0 \{\cos \theta - \cos(\omega t + \theta)\}$, where γ_0 , ω , and θ are the strain amplitude, the angular frequency, and the initial phase, respectively. For the initial $N_c^{(I)}$ cycles, we use $\gamma_0 = \gamma_0^{(I)}$ with the initial strain amplitude $\gamma_0^{(I)}$. After the initial shear, we apply the oscillatory shear with much small strain amplitude $\gamma_0 = \gamma_0^{(F)}$ for $N_c^{(F)}$ cycles, and measure the storage and the loss moduli in the final cycle defined by [66]

$$G' = -\frac{\omega}{\pi} \int_0^{2\pi/\omega} dt \sigma(t) \cos(\omega t + \theta) / \gamma_0^{(F)}, \quad (1)$$

$$G'' = \frac{\omega}{\pi} \int_0^{2\pi/\omega} dt \sigma(t) \sin(\omega t + \theta) / \gamma_0^{(F)}. \quad (2)$$

The shear stress σ is given by

$$\sigma = -\frac{1}{L^2} \sum_i \sum_{j>i} (r_{i,x} - r_{j,x}) F_{ij,y}(t), \quad (3)$$

where $r_{i,\alpha}$ is the α -component of the position vector of the grain i , and $F_{ij,\beta}$ is the β component of the contact force between grain i and grain j . Here, we have ignored the kinetic part of σ because it is significantly smaller than the potential part for highly dissipative grains. We have mainly used $N_c^{(I)} = N_c^{(F)} = 10$, and confirmed that the value of G' is identical to that for $N_c^{(I)} = N_c^{(F)} = 1000$ within error bars. Note that G' and the dynamic viscosity $\eta \equiv G''/\omega$ are almost independent of ω and $\gamma_0^{(F)}$ for $\omega \leq 10^{-2}\tau^{-1}$ and $\gamma_0^{(F)} \leq 10^{-3}$, where $\tau = \sqrt{m_0/k^{(n)}}$ is the characteristic time of the stiffness with the mass m_0 for a grain of diameter d_0 [61]. We, thus, focus on the dependence of the shear modulus only on $\gamma_0^{(I)}$ and ϕ for $\omega = 10^{-4}\tau^{-1}$ and $\gamma_0^{(F)} = 10^{-4}$. Here, the dynamic viscosity $\eta(\omega)$ is almost identical to the shear viscosity $\eta(0)$ [66]. We mainly use $N = 4000$, $k^{(t)} = 0.2k^{(n)}$, $\eta^{(t)} = \eta^{(n)} = \sqrt{m_0k^{(n)}}$, and $\mu = 1.0$. This set of parameters corresponds to the constant restitution coefficient $e = 0.043$. Note that we have estimated the isotropic transition point $\phi_J = 0.822$. See Supplement Materials [67] for the μ -dependence of our numerical results. We have also confirmed that G' for $N = 16000$ is almost identical to that for $N = 4000$ within the error bars. We adopt the leapfrog algorithm with the time step $\Delta t = 0.05\tau$.

Mechanical response. – In Fig. 1, we plot the force chain network after the initial oscillatory shear for $\phi = 0.820 < \phi_J$ and $\theta = 0$ with $\gamma_0^{(I)} = 0.1, 0.12$ and 1.0 . For small initial strain amplitude ($\gamma_0^{(I)} = 0.1$), the system stays in a

liquid-like state without percolating force chain networks. For $\gamma_0^{(I)} = 0.12$ and 1.0 , however, the systems have percolating force chain networks, where the network might be anisotropic for $\gamma_0^{(I)} = 0.12$

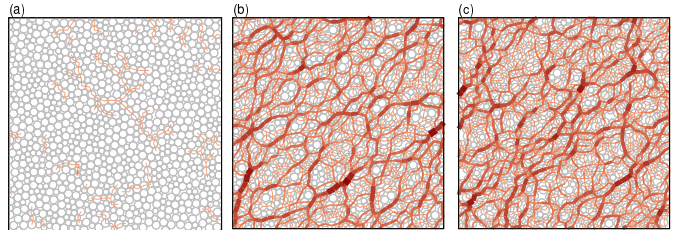


FIG. 1: (Color online) Snapshots of grains (circles) and force chains (lines) after the initial oscillatory shear for $\phi = 0.820$ and $\theta = 0$ with (a) $\gamma_0^{(I)} = 0.1$, (b) 0.12 , and (c) 1.0 . The color and the width of each line depends on the absolute value of the interaction force between grains.

Figure 2 exhibits the transition of the mechanical response associated with the shear jamming, where G' is plotted against $\gamma_0^{(I)}$ for $\theta = 0$ and $\pi/2$ with $\phi = 0.820$. G' changes from 0 to a finite value at a critical strain amplitude γ_S around $\gamma_0^{(I)} = 0.12$. The value of γ_S , however, depends on θ , and the solid-like state with $G' > 0$ and the liquid-like states with $G' \simeq 0$ coexist in the shaded region of Fig. 2 as a metastable state. The inset of Fig. 2 exhibits the storage modulus G' against θ for $\phi = 0.82$ with $\gamma_0^{(I)} = 0.12$, which indicates that G' in the metastable state has peaks at $n\pi$ and becomes 0 near $(n + 1/2)\pi$ with an integer n . See Supplement Materials for the stress-strain curves showing the onset of the shear jamming and the θ -dependence in the metastable state [67].

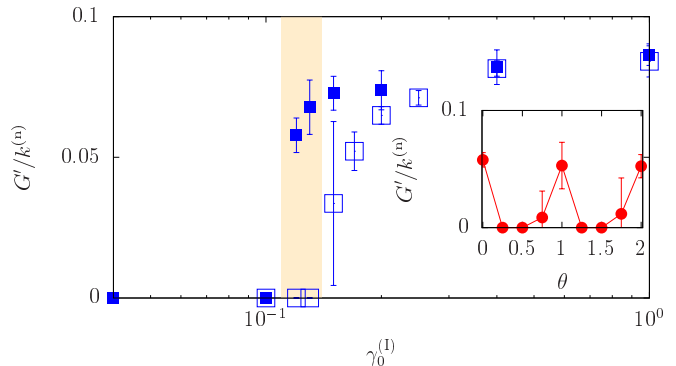


FIG. 2: (Color online) The storage modulus G' against $\gamma_0^{(I)}$ for $\phi = 0.82$ with $\theta = 0$ and $\pi/2$. The shaded region indicates the fragile state. Inset: The storage modulus G' against θ for $\phi = 0.82$ with $\gamma_0^{(I)} = 0.12$

In Fig. 3, we plot G' against $\gamma_0^{(I)}$ for various ϕ with $\theta = 0$. For $\phi > \phi_J$, G' is finite for any $\gamma_0^{(I)}$, but G' depends on $\gamma_0^{(I)}$. The decrease of G' for $\phi > 0.84$ is

similar to softening observed in glassy materials under steady shear [68]. We identify the existence of the shear jamming for $\phi_C < \phi < \phi_J$ with $\phi_C = 0.794$.

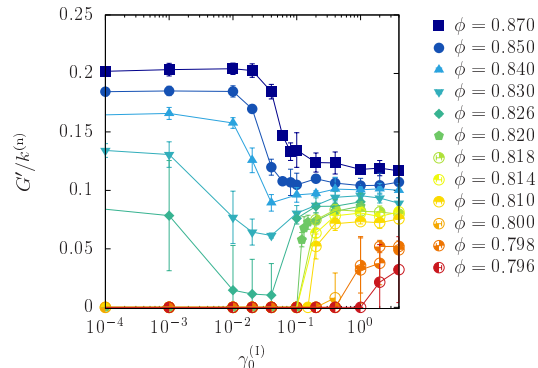


FIG. 3: (Color online) The storage modulus G' against $\gamma_0^{(1)}$ for various ϕ with $\theta = 0$.

Figure 4 plots the dimensionless η against $\gamma_0^{(1)}$ for $\theta = 0$ with various ϕ . For $\phi > \phi_J$, η is almost independent of $\gamma_0^{(1)}$, while η for $\phi_C < \phi < \phi_J$ exhibits a sudden increase from a negligibly small value to a larger value at γ_S . The sudden increase of η is similar to the DST under steady shear.

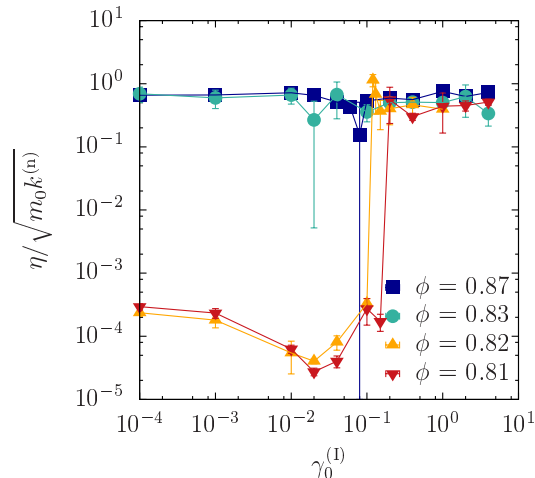


FIG. 4: (Color online) The dynamic viscosity η against the initial strain amplitude $\gamma_0^{(1)}$ for $\theta = 0$ with various ϕ .

Phase diagram.— Figure 5 illustrates a phase diagram on the plain of $\gamma_0^{(1)}$ and ϕ . Here, we introduce the shear storage modulus without the initial oscillatory shear: $G'_0(\phi) \equiv \lim_{\gamma_0^{(1)} \rightarrow 0} G'(\phi, \gamma_0^{(1)})$. Then, we define the jammed state (J) as the region where $G'_0(\phi) > G_{\text{th}}$ for any θ with a sufficiently small threshold $G_{\text{th}} = 10^{-4}k^{(n)}$. Note that the phase diagram is unchanged if we use $G_{\text{th}} = 10^{-5}k^{(n)}$. The unjammed state (U) is defined as $G'_0(\phi, \gamma_0^{(1)}) < G_{\text{th}}$ for any θ . The shear jammed state (SJ) is defined as $G'_0(\phi) < G_{\text{th}}$ and $G'(\phi, \gamma_0^{(1)}) > G_{\text{th}}$ for any

θ . Finally, we define the fragile state (F) as the solid-like state with $G'(\phi, \gamma_0^{(1)}) > G_{\text{th}}$ and the liquid-like state with $G'(\phi, \gamma_0^{(1)}) < G_{\text{th}}$ coexist as shown in Fig. 2. In Fig. 5, we present the phase diagram based on our simulation. SJ exists only for $\phi_C < \phi < \phi_J$ and $\gamma_0^{(1)} > 0.1$. We have also confirmed that F exists between U and SJ.

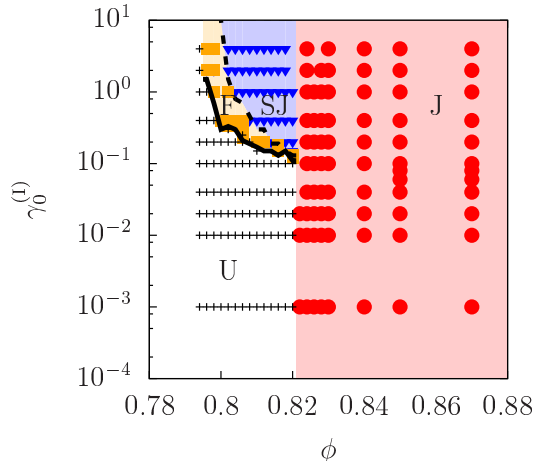


FIG. 5: (Color online) The phase diagram showing the different states: jammed state (circles), shear jammed state (triangles), fragile state (squares), and unjammed state (crosses). The solid and the dashed lines are the critical strain γ_S for $\theta = 0$ and $\pi/2$, respectively.

In Fig. 5, we also plot the critical strain γ_S estimated from the DST-like behavior, where η exceeds a threshold $10^{-3}\sqrt{m_0 k^{(n)}}$. The critical strain γ_S for $\theta = 0$ exists on the boundary between U and F, while γ_S for $\theta = \pi/2$ is on the boundary between F and SJ. We also find that γ_S for various values of θ lies in the fragile state. This suggests that the region of the fragile state is identical to that for the DST-like behavior.

Discussion and concluding remarks.— Let us discuss our results. Recent numerical simulations [69–78] indicate that the shear jamming can be observed even in frictionless systems. However, the observation of SJ in frictionless systems needs special protocols [69–72], small system sizes [73–75], or the modification of the contact between grains [76–78]. These results suggest that SJ in frictionless systems is unstable. This is consistent with the μ -dependence of our results shown in Supplement Materials [67].

The fragile state is originally defined by the anisotropic percolation of the force network under quasi-static pure shear process [32]. Note that there is neither specific compression direction nor quasi-static operations in our system, and the anisotropy of the force chain network in our fragile state (Fig. 1) is not clear. Nevertheless, we have confirmed that stress anisotropy τ/P , which is also characterize the onset of the shear jamming [58, 75], exhibits the maximum in the fragile state as shown in Fig. 6, where $\tau = (\sigma_1 - \sigma_2)/2$ and $P = (\sigma_1 + \sigma_2)/2$ with the maximum and the minimum principal stresses σ_1 and σ_2 ,

respectively. We should note that the DST is originally defined by the jump of the viscosity against the shear rate [40], while our DST-like behavior is the discontinuous jump when we control the initial strain amplitude $\gamma_0^{(1)}$. Further careful study on the mutual relationship should be necessary.

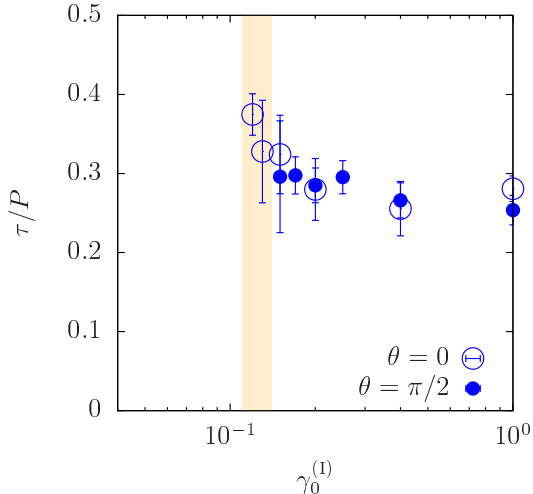


FIG. 6: (Color online) The stress anisotropy τ/P against $\gamma_0^{(1)}$ for $\phi = 0.820$ with $\theta = 0$ and $\pi/2$. The shaded region indicates the fragile state.

In conclusion, we have numerically studied the frictional granular systems under oscillatory shear. Controlling the strain amplitude of the oscillatory shear before the measurement, we find that the shear jamming is regarded as the protocol dependent state in which the shear jammed state only appears above a critical strain amplitude. This protocol dependent behavior can be used to detect the DST-like behavior, where the viscosity exhibits a discontinuous jump against the initial strain amplitude. The region where the DST-like behavior is observed coincides with the fragile state, where the liquid-like state and the solid-like states coexist. Our results clarify properties of shear induced exotic states in granular materials.

The authors thank C. S. O'Hern, C. Maloney, B. Chakraborty, R. Behringer, S. Sastry, H. A. Vinutha, T. Kawasaki, K. Saito, and S. Takada for fruitful discussions. This work is partially supported by the Grant-in-Aid of MEXT for Scientific Research (Grant No. 16H04025 and No. 17H05420). One of the authors (M.O.) appreciates the warm hospitality of Yukawa Institute for Theoretical Physics at Kyoto University during his stay there supported by the Program No. YITP-W-15-19.

-
- [1] A. J. Liu and S. R. Nagel, *Nature* **396**, 21 (1998).
 - [2] M. van Hecke, *J. Phys.: Condens. Matter* **22**, 033101 (2009)
 - [3] R. P. Behringer and B. Chakraborty, *Rep. Prog. Phys.* in press.
 - [4] C. S. O'Hern, S. A. Langer, A. J. Liu, and S. R. Nagel, *Phys. Rev. Lett.* **88**, 075507 (2002).
 - [5] C. S. O'Hern, L. E. Silbert, A. J. Liu, and S. R. Nagel, *Phys. Rev. E* **68**, 011306 (2003).
 - [6] M. Wyart, *Annales de Physique* **30**, 3 (2005).
 - [7] P. Olsson and S. Teitel, *Phys. Rev. Lett.* **99**, 178001 (2007).
 - [8] T. Hatano, M. Otsuki, and S. Sasa, *J. Phys. Soc. Jpn.* **76**, 023001 (2007).
 - [9] T. Hatano, *J. Phys. Soc. Jpn.* **77**, 123002 (2008).
 - [10] B. P. Tighe, E. Woldhuis, J. J. C. Remmers, W. van Saarloos, and M. van Hecke, *Phys. Rev. Lett.* **105**, 088303 (2010).
 - [11] T. Hatano, *Prog. Theor. Phys. Suppl.* **184**, 143 (2010).
 - [12] M. Otsuki and H. Hayakawa, *Prog. Theor. Phys.* **121**, 647 (2009).
 - [13] M. Otsuki and H. Hayakawa, *Phys. Rev. E* **80**, 011308 (2009).
 - [14] M. Otsuki, H. Hayakawa, and S. Luding, *Prog. Theor. Phys. Suppl.* **184**, 110 (2010).
 - [15] K. N. Nordstrom, E. Verneuil, P. E. Arratia, A. Basu, Z. Zhang, A. G. Yodh, J. P. Gollub, and D. J. Durian, *Phys. Rev. Lett.* **105**, 175701 (2010).
 - [16] P. Olsson and S. Teitel, *Phys. Rev. E* **83**, 030302(R) (2011).
 - [17] D. Vågberg, P. Olsson, and S. Teitel, *Phys. Rev. E* **83**, 031307 (2011).
 - [18] M. Otsuki and H. Hayakawa, *Prog. Theor. Phys. Suppl.* **195**, 129 (2012).
 - [19] A. Ikeda, L. Berthier, and P. Sollich, *Phys. Rev. Lett.* **109**, 018301 (2012).
 - [20] P. Olsson and S. Teitel, *Phys. Rev. Lett.* **109**, 108001 (2012).
 - [21] E. DeGiuli, G. Düring, E. Lerner, and M. Wyart, *Phys. Rev. E* **91**, 062206 (2015).
 - [22] D. Vågberg, P. Olsson, and S. Teitel *Phys. Rev. E* **93**, 052902 (2016).
 - [23] F. Boyer, E. Guazzelli, and O. Pouliquen, *Phys. Rev. Lett.* **107**, 188301 (2011).
 - [24] M. Trulsson, B. Andreotti, and P. Claudin, *Phys. Rev. Lett.* **109**, 118305 (2012).
 - [25] B. Andreotti, J.-L. Barrat, and C. Heussinger, *Phys. Rev. Lett.* **109**, 105901 (2012).
 - [26] E. Lerner, G. Düring, and M. Wyart, *Proc. Natl. Acad. Sci. U.S.A* **109**, 4798 (2012).
 - [27] D. Vågberg, P. Olsson, and S. Teitel *Phys. Rev. Lett.* **113**, 148002 (2014).
 - [28] T. Kawasaki, D. Coslovich, A. Ikeda, and L. Berthier, *Phys. Rev. E* **91**, 012203 (2015).
 - [29] K. Suzuki and H. Hayakawa, *Phys. Rev. Lett.* **115**, 098001 (2015).
 - [30] B. P. Tighe, *Phys. Rev. Lett.* **107**, 158303 (2011).
 - [31] M. Otsuki and H. Hayakawa, *Phys. Rev. E* **90**, 042202 (2011).

- (2014).
- [32] D. Bi, J. Zhang, B. Chakraborty and R. Behringer, Nature **480**, 355 (2011).
- [33] J. Zhang, T. Majmudar, and R. Behringer, Chaos **18**, 041107 (2008).
- [34] J. Zhang, T. Majmudar, A. Tordesillas, and R. Behringer, Granular Matter **12**, 159 (2010).
- [35] D. Wang, J. Ren, J. A. Dijksman, H. Zhen, and R. Behringer, Phys. Rev. Lett. **120**, 208004 (2018).
- [36] S. Sarkar, D. Bi, J. Zhang, R. Behringer and B. Chakraborty, Phys. Rev. Lett. **111**, 068301 (2013).
- [37] S. Sarkar, D. Bi, J. Zhang, J. Ren, R. Behringer and B. Chakraborty, Phys. Rev. E **93**, 042901 (2016).
- [38] M. Otsuki and H. Hayakawa, Phys. Rev. E **83**, 051301 (2011).
- [39] S. Chialvo, J. Sun, and S. Sundaresan, Phys. Rev. E **85**, 021305 (2012).
- [40] E. Brown and H. M. Jaeger, Phys. Rev. Lett. **103**, 086001 (2009).
- [41] R. Seto, R. Mari, J. F. Morris, and M. M. Denn, Phys. Rev. Lett. **111**, 218301 (2013).
- [42] N. Fernandez, R. Mani, D. Rinaldi, D. Kadau, M. Mosquet, H. Lombois-Burger, J. Cayer-Barrioz, H. J. Herrmann, N. D. Spencer, and L. Isa, Phys. Rev. Lett. **111**, 108301 (2013).
- [43] C. Heussinger, Phys. Rev. E **88**, 050201 (2013).
- [44] M. M. Bandi, M. K. Rivera, F. Krzakala and R.E. Ecke, Phys. Rev. E **87**, 042205 (2013).
- [45] M. P. Ciamarra, R. Pastore, M. Nicodemi, and A. Coniglio, Phys. Rev. E **84**, 041308 (2011).
- [46] R. Mari, R. Seto, J. F. Morris, and M. M. Denn, J. Rheol. **58**, 1693 (2014).
- [47] M. Grob, C. Heussinger, and A. Zippelius, Phys. Rev. E **89**, 050201(R) (2014).
- [48] T. Kawasaki, A. Ikeda, and L. Berthier, EPL **107**, 28009 (2014).
- [49] M. Wyart and M. E. Cates, Phys. Rev. Lett. **112**, 098302 (2014).
- [50] M. Grob, A. Zippelius, and C. Heussinger, Phys. Rev. E **93**, 030901(R) (2016).
- [51] H. Hayakawa and S. Takada, arXiv:1611.07925.
- [52] H. Hayakawa, S. Takada, and V. Garzo, Phys. Rev. E **96**, 042903 (2017).
- [53] I. R. Peters, S. Majumdar, and H. M. Jaeger, Nature **532**, 214 (2017).
- [54] A. Fall, F. Bertrand, D. Hautemayou, C. Mezière, P. Moucheron, A. Lemaître, and G. Ovarlez, Phys. Rev. Lett. **114**, 098301 (2015).
- [55] S. Sarkar, E. Shatoff, K. Ramola, R. Mari, J. Morris, and B. Chakraborty, EPJ Web conf. **140**, 09045 (2017).
- [56] A. Singh, R. Mari, M. M. Denn, and J. F. Morris, J. J. Rheol. **62**, 457 (2018).
- [57] T. Kawasaki and L. Berthier, Phys. Rev. E **98**, 012609 (2018).
- [58] J. E. Thomas, K. Ramola, A. Singh, R. Mari, J. Morris, and B. Charkraborty, Phys. Rev. Lett. **112**, 128002 (2018).
- [59] E. Somfai, M. van Hecke, W. G. Ellenbroek, K. Shundyak, and W. van Saarloos, Phys. Rev. E **75**, 020301(R) (2007).
- [60] V. Magnanimo, L. La Ragione, J. T. Jenkins, P. Wang, and H. A. Makse, EPL **81**, 34006 (2008).
- [61] M. Otsuki and H. Hayakawa, Phys. Rev. E **96**, 062902 (2017).
- [62] E. Brown and H. M. Jaeger, Rep. Prog. Phys. **77**, 046602 (2014).
- [63] E. Brown, N. Rodenberg, J. Amend, A. Mozeika, E. Steltz, M. R. Zakin, H. Lipson, and H. M. Jaeger, Proc. Natl. Acad. Sci. U.S.A **107**, 18809 (2010).
- [64] P. Cundall and O. D. L. Strack, Geotechnique **29**, 47 (1979).
- [65] D. J. Evans and G. P. Morriss, *Statistical Mechanics of Nonequilibrium Liquids* 2nd ed. (Cambridge University Press, Cambridge, 2008).
- [66] M. Doi and S. F. Edwards, *The Theory of Polymer Dynamics* (Oxford University Press, Oxford, 1990).
- [67] See Supplemental Material.
- [68] M. Fan, K. Zhang, J. Schroers, M. D. Shattuck, and C. S. O'Hern, Phys. Rev. E **96**, 032602 (2017).
- [69] N. Kumar and S. Luding, Granul. Matter **18**, 58 (2016).
- [70] Y. Jin and H. Yoshino, Nat. Commun. **118**, 14935 (2017).
- [71] P. Urbani and F. Zamponi, Phys. Rev. Lett. **118**, 038001 (2017).
- [72] Y. Jin, P. Uvbani, F. Zamponi, and H. Yoshino, arXiv:1803.04597.
- [73] T. Bertrand, R. Behringer, B. Chakraborty, C. S. O'Hern, and M. D. Shattuck, Phys. Rev. E **93**, 012901 (2016).
- [74] M. Baity-Jesi, C. P. Goodrich, A. J. Liu, S. R. Nagel, and J. P. Sethna, J. Stat. Phys. **167**, 735 (2017).
- [75] S. Chen, W. Jin, T. Bertrand, M. D. Shattuck, and C. O'Hern, arXiv:1804.10962.
- [76] H. A. Vinutha and S. Sastry, Nat. Phys. **12**, 578 (2016).
- [77] H. A. Vinutha and S. Sastry, J. Stat. Mech. **2016**, 094002 (2016).
- [78] H. A. Vinutha and S. Sastry, arXiv:1705.10109.

Supplemental Materials:

I. SUMMARY

In this Supplemental Materials, we present the stress-strain curve associated with the shear jamming, and the dependence of the phase diagram on the friction coefficient μ .

II. STRESS-STRAIN CURVE ASSOCIATED WITH SHEAR JAMMING

In this section, we show the stress-strain curves to illustrate how the shear jamming takes place in the initial oscillatory shear and demonstrate the effect of the initial phase θ in the fragile state. In Fig. S1, we plot the shear stresses σ against the strain γ for $\gamma_0^{(I)} = 0$ and 0.2 with $\gamma_0^{(F)} = 0.01$ at $\phi = 0.820$ and $\theta = 0$. Note that $\gamma_0^{(I)} = 0$ and 0.2 correspond to the unjammed and the shear jammed states, respectively. Without the initial shear ($\gamma_0^{(I)} = 0$), σ remains 0 in the oscillatory shear with $\gamma_0^{(F)} = 0.01$ as shown in the bold blue line. On the other hand, σ follows a stress-strain loop under the initial oscillatory shear with $\gamma_0^{(I)} = 0.2$ once γ exceeds $\gamma \simeq 0.02$. Then, the stress σ remains finite and exhibits a linear increase even when we measure the shear modulus with $\gamma^{(F)} = 0.01$ as shown in the red dashed line, which indicates $G' > 0$ corresponding to the shear jamming.

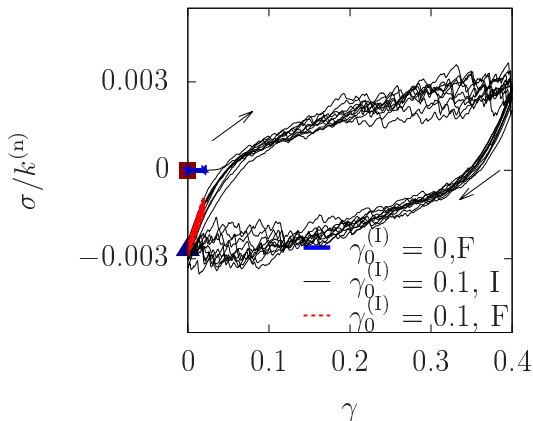
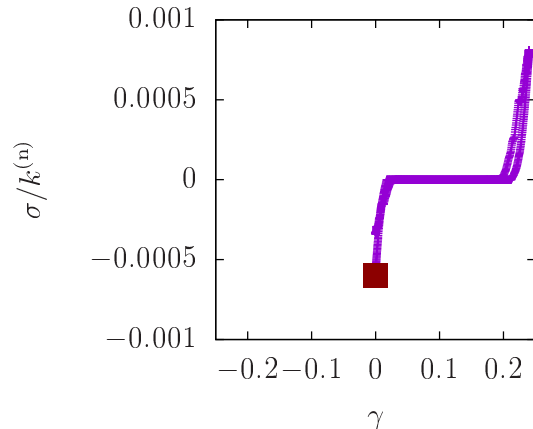


FIG. S1: (Color online) The shear stress σ against the strain γ with $\gamma_0^{(I)} = 0.0$ and 0.2 for $\gamma_0^{(F)} = 0.01$, $\phi = 0.820$, and $\theta = 0$. "I" and "F" denote the results for the initial oscillatory shear and the final oscillatory shear to the measure mechanical properties, respectively. The square and the triangle indicate the states before and after the initial oscillatory shear for $\gamma_0^{(I)} = 0.2$, respectively. The arrows demonstrate the evolution of σ .

Figure S2 illustrates the shear stress σ against the strain γ in the final cycle of the initial oscillatory with

$\gamma_0^{(I)} = 1.2$ and $\phi = 0.820$ for $\theta = 0$ and $\pi/2$. For $\theta = 0$, σ exhibits an almost linear response against γ near the maximum and the minimum values of γ , while σ remains 0 for $0.03 < \gamma < 0.2$. After the initial oscillatory shear, the mechanical response of the system is solid-like i.e. with $G' > 0$ near $\gamma \approx 0$. For $\theta = \pi/2$, the qualitative behavior is almost identical to that for $\theta = 0$ except for the the maximum and the minimum values of γ . After the initial oscillatory shear, the response for $\theta = \pi/2$ is liquid-like near $\gamma \approx 0$, i.e. $G' = 0$. These behaviors explain the dependence of G' on θ shown in Fig. 2.

(a)



(b)

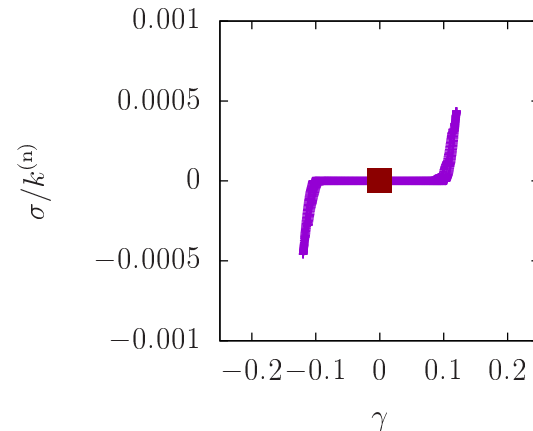


FIG. S2: (Color online) The shear stress σ against the strain γ in the last cycle of the initial oscillatory with $\gamma_0^{(I)} = 0.12$ at $\phi = 0.820$ for $\theta = 0$ (a) and $\pi/2$ (b). The solid square indicates the state just after the initial oscillatory shear.

III. DEPENDENCE OF TRANSITION POINTS ON μ

In this section, we show the dependence on the friction coefficient μ . In Fig. S3, we plot the critical point ϕ_J for isotropic jamming and the minimum value ϕ_C for SJ.

Note that SJ exists between ϕ_C and ϕ_J . As shown in Fig. S3, the difference between ϕ_J and ϕ_C decreases as μ decreases. Then, ϕ_C becomes identical to ϕ_J in the limit $\mu \rightarrow 0$, which indicates that SJ disappears in the frictionless limit.

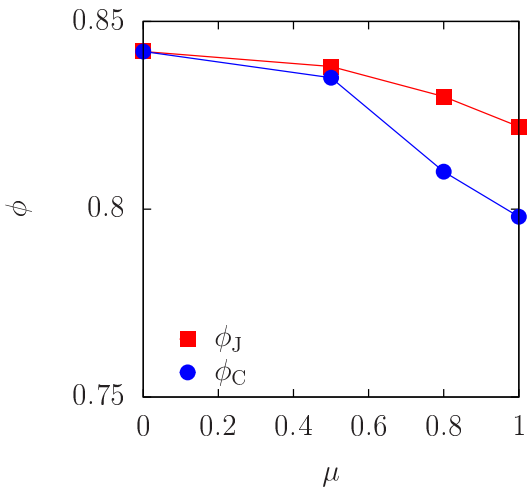


FIG. S3: (Color online) The transition points ϕ_J and ϕ_C against μ .